

DOCUMENT CONTROL SHEET

	ORIGINATOR'S REF. NLR TP 96523 U		SECURITY CLASS. Unclassified										
ORIGINATOR National Aerospace Laboratory NLR, Amsterdam, The Netherlands													
TITLE Influence of blade rotation on the sectional aerodynamics of rotational blades													
PRESENTED AT The twenty-second European Rotorcraft Forum, September 17-19, 1996, Brighton, United Kingdom.													
AUTHORS J. Bosschers, B. Montgomerie, A.J. Brand, R.P.J.O.M. van Rooy		DATE 960823	pp ref 23 32										
DESCRIPTORS <table style="width: 100%; border: none;"> <tr> <td style="width: 50%;">Computer programs</td> <td style="width: 50%;">Rotor blades</td> </tr> <tr> <td>Lift</td> <td>Rotor aerodynamics</td> </tr> <tr> <td>Prediction analysis techniques</td> <td>Separated flow</td> </tr> <tr> <td>Pressure distribution</td> <td>Three dimensional boundary layer</td> </tr> <tr> <td>Rotation</td> <td>Wind turbines</td> </tr> </table>				Computer programs	Rotor blades	Lift	Rotor aerodynamics	Prediction analysis techniques	Separated flow	Pressure distribution	Three dimensional boundary layer	Rotation	Wind turbines
Computer programs	Rotor blades												
Lift	Rotor aerodynamics												
Prediction analysis techniques	Separated flow												
Pressure distribution	Three dimensional boundary layer												
Rotation	Wind turbines												
ABSTRACT It is known that due to rotation of the blade, lift coefficients on inboard sections may exceed the 2-D maximum lift coefficient. A model to take into account was suggested by Snel (25). Initial calculations with this model were reported by Snel and Houwink (27). The model is further analysed and implemented in a 2-D viscous-inviscid interaction code, with a panel method for the inviscid flow, and an integral method for the boundary layer. Calculated pressure distributions and lift coefficients are compared with experimental data and with the previously obtained results using a different 2-D flow solver. The two codes capture the effects of blade rotation, but overpredict the increase in lift. The effect of Reynolds number and rotational speed is discussed, as well as the influence of transition on lift, drag and moment coefficient. A calculation will be presented showing the influence of blade rotation on a pitching airfoil in light stall.													

NLR TECHNICAL PUBLICATION



TP 96523 U

INFLUENCE OF BLADE ROTATION ON THE SECTIONAL
AERODYNAMICS OF ROTATIONAL BLADES

by

J. Bosschers, B. Montgomerie,
A.J. Brand, R.P.J.O.M. van Rooy

This paper has been presented at the twenty-second European Rotorcraft Forum, September 17-19, 1996, Brighton, United Kingdom.

Division : Fluid Dynamics
Prepared : JB/ 
Approved : RJZ/ 

Completed : 960823
Order number : 024.022
Typ. : LMT



Contents

Abstract	5
1 Nomenclature	5
2 Introduction	5
3 3-D boundary layer equations	6
3.1 Order of magnitude analysis	7
3.1.1 Attached flow	7
3.1.2 Separated flow	7
3.2 Nondimensional equations	7
3.3 Exact solutions	8
4 Implementation in VII codes	9
5 Steady calculations	10
5.1 Influence of blade rotation	10
5.2 Influence of higher order terms	10
5.3 Comparison with experiment	10
5.4 Comparison with Navier-Stokes results	11
5.5 Influence on lift	11
5.6 Influence of velocity variation	11
5.7 Influence of transition	12
6 Unsteady calculations	12
7 Concluding remarks	12
8 References	13
17 Figures	

(23 pages in total)



This page is intentionally left blank

Influence of blade rotation on the sectional aerodynamics of rotating blades

J. Bosschers
National Aerospace
Laboratory NLR
Amsterdam
the Netherlands

B. Montgomerie and A.J. Brand
Netherlands Energy Research
Foundation ECN
Petten
the Netherlands

R.P.J.O.M. van Rooy
Institute for Wind Energy,
Delft University of Technology
Delft
the Netherlands

Abstract

It is known that due to rotation of the blade, lift coefficients on inboard sections may exceed the 2-D maximum lift coefficient. A model to take this into account was suggested by Snel [25]. Initial calculations with this model were reported by Snel and Houwink [27]. The model is further analysed and implemented in a 2-D viscous-inviscid interaction code, with a panel method for the inviscid flow, and an integral method for the boundary layer. Calculated pressure distributions and lift coefficients are compared with experimental data and with the previously obtained results using a different 2-D flow solver. The two codes capture the effects of blade rotation, but overpredict the increase in lift. The effect of Reynolds number and rotational speed is discussed, as well as the influence of transition on lift, drag and moment coefficient. A calculation will be presented showing the influence of blade rotation on a pitching airfoil in light stall.

1. Nomenclature

c	chord
f_0	nondimensional free-stream velocity: $f_0 = W/\Omega r$
p	pressure
q	velocity vector (u,v,w)
r	radius in cylindrical coordinate system
s	arc length in cylindrical coordinate system
u,v,w	velocity components in cylindrical coordinate system (θ, r, z)
z	height normal to airfoil chord, cylindrical coordinate system
A	cross-flow parameter
C_d	drag coefficient
C_l	lift coefficient
C_m	moment coefficient
C_f	skin friction coefficient
C_p	pressure coefficient
H	shape factor, $H = \delta^*/\theta$
H_1	Head's shape factor, $H_1 = (\delta - \delta^*)/\theta$
M	Mach number
R.	tip radius
Re	Reynolds number ($= \rho Wc/\mu$)

Ro Rossby number ($= f_0 r/c$)
W effective wind speed as seen by blade section

Greek

α angle of attack
 β streamline angle
 δ boundary layer thickness
 δ^* boundary layer displacement thickness
 θ (i) boundary layer momentum thickness
(ii) angle in cylindrical coordinate system
 λ tip speed ratio ($= \Omega R/W$)
 μ molecular viscosity
 ρ density
 Ω angular velocity

Subscripts

e boundary layer edge
w at the wall
1 in θ (chordwise) direction
2 in radial direction

2. Introduction

Blade element theory is often used to calculate the performance and aeroelastic behaviour of wind turbines and helicopters. Use is made of 2-D aerofoil data, supplemented with correction methods for unsteady effects, 3-D effects and Reynolds number effects. A 3-D effect of importance for (stall-regulated) wind turbines, tilt rotors and highly loaded helicopter rotors is the increase in maximum lift at sections located near the hub due to the rotation of the blade.

The influence of blade rotation was first investigated by Himmelskamp (see Schlichting [24]), who measured very large lift coefficients, beyond the 2-D steady maximum lift coefficient, on a rotating propeller. The effect was attributed to the presence of a Coriolis force, having the same effect as a favourable pressure gradient. In addition, the centrifugal force causes an outward displacement of fluid particles, through which the boundary layer becomes thinner compared to a non-rotating boundary layer.

Fogarty [9] calculated the laminar boundary layer on a



rotating blade in attached flow. He concluded that differences compared to a non-rotating blade were small, but remarked that the situation may differ for separated flow. Experimental data up to 1973 was summarized by McCroskey [16]. In separated flow large skew angles (angle between surface streamline and circular arc) were measured, and for attached flow small angles. Laminar attached flow showed larger skew angles than turbulent attached flow.

More recent measurements on wind turbine blades showing a large increase in lift at the inboard sections were reported by Bruining et al. [6], Ronsten [22] and Paynter & Graham [20].

At ECN both non-rotating and rotating measurements have been made on a field rotor by Brand et al. [5]. Results for the rotating case ($Re = 2.1 \text{ E}6$, NACA 4424 airfoil) at zero yaw angle of the rotor axis are seen in figure 1. Here an absence in maximum normal force is seen in stall on the inboard section for most negative pitch angles, but for the positive pitch angles results are quite different. No satisfactory explanation could be given so far for this pitch dependency. The increase in normal force was also influenced by the yaw angle of the wind turbine rotor axis.

3-D calculations on a wind turbine blade showing the increase in maximum lift explained by a delay of flow separation due to Coriolis forces were made by Sørensen [28] using a 3-D viscous-inviscid interaction method. These results were confirmed by an analysis using Navier-Stokes calculations by Narramore & Vermeland [19] on a tilt rotor blade in stall. Hansen [10] used a 3-D Navier-Stokes method to analyse the flow over wind turbine blades in stall, and compared his results with 2-D calculated results, clearly showing the increase in sectional lift coefficients at inboard stations due to blade rotation.

In order to include the increase in lift due to blade rotation in blade element codes, empirical correction methods have been developed. Corrigan and Schillings [7] present a stall delay angle of attack formulation based upon the results of Banks and Gadd [2]. Bessone and Petot [3] show the increase in lift at the retreating side of a highly loaded helicopter rotor in fast forward flight using a correction model for blade rotation based upon the results of Snel and Houwink [27].

The work described here is a continuation of the model developed by Snel [25] and Snel and Houwink [27]. Following an order of magnitude analysis of the 3-D boundary layer equations, leading terms could be identified in attached and separated flow. Neglecting higher order terms resulted in a system of equations which could be implemented in a 2-D flow solver, while still retaining the essential terms due to blade rotation. The flow solver was based upon a viscous-inviscid interaction method. The inviscid flow was considered 2-D. The principal parameter to determine blade rotational effects is the local chord divided by section radius, c/r . The model predicted qualitatively the de-

lay in separation and increase in lift on inboard sections, but a correction had to be applied upon the c/r parameter in order to obtain the same increase in lift as measured. With this tuned model, a simple correction method for use in blade element based computer codes was then devised to take rotational effects into account on wind turbine blades. Using this correction method, given also in this paper, the power prediction of wind turbines was improved.

However, because the so-called Snel model for blade rotation lacked quantitative correlation with experiment, a cooperation between ECN, TU Delft and NLR was started to improve this. Two steps were proposed: Implementation in a computer code more suited for wind turbine airfoils which is used in the Dutch wind energy community, and extension of the model with higher order terms. The TU Delft [31] improved the lift prediction and convergence behaviour of the code, NLR implemented the Snel model, and ECN will analyse and validate calculations with the goal of deriving a more accurate correction formula for the effect of blade rotation. The project was financed by NOVEM. General results have been presented by Montgomerie [17].

The present paper will discuss some of the NLR results obtained in this project and in the EC DGXII Joule II project "Dynamic Stall and Three-Dimensional Effects", which was partly financed by NOVEM. First the order of magnitude analysis will be reviewed, after which some aspects of the resulting equations will be discussed. Calculations will be compared with measurements and the Navier-Stokes calculations of Hansen [10]. The influence of Reynolds number and wind speed will be shown. All results have been calculated with fixed transition at the leading edge. When transition is not fixed, it might be enhanced by the cross-flow. Therefore the influence of transition on lift, drag and moment coefficient will be discussed briefly. Finally unsteady calculations with and without the blade rotational effects will be shown.

3. 3-D boundary layer equations

The incompressible boundary layer equations for a rotating blade, using a cylindrical axis system attached to the blade [32], figure 2, are the continuity equation:

$$\frac{\partial u}{r \partial \theta} + \frac{v}{r} + \frac{\partial v}{\partial r} + \frac{\partial w}{\partial z} = 0, \quad (1)$$

the θ momentum equation:

$$u \frac{\partial u}{r \partial \theta} + v \frac{\partial u}{\partial r} + w \frac{\partial u}{\partial z} = q_e \frac{\partial q_e}{r \partial \theta} + \frac{\mu}{\rho} \frac{\partial^2 u}{\partial z^2} + 2\Omega v - \frac{uv}{r}, \quad (2)$$

and the r momentum equation:

$$u \frac{\partial v}{r \partial \theta} + v \frac{\partial v}{\partial r} + w \frac{\partial v}{\partial z} = q_e \frac{\partial q_e}{\partial r} + \frac{\mu}{\rho} \frac{\partial^2 v}{\partial z^2} + \frac{u}{r} (u - 2\Omega r). \quad (3)$$

In the θ momentum equations the Coriolis term is given by $2\Omega v$, in the r momentum equation it is given by $2\Omega u$. The pressure gradient has been eliminated from the equations using the Bernoulli equation, which reads for a rotating coordinate system:

$$\text{grad} \left| \frac{q_e^2}{2} \right| - \text{grad} \frac{(\Omega r)^2}{2} = -\frac{1}{\rho_e} \text{grad} p_e. \quad (4)$$

3.1 Order of magnitude analysis

The order of magnitude analysis of Fogarty [9] for attached flow, and of Snel [25] for separated flow is briefly reviewed here.

3.1.1 Attached flow

For attached flow it is assumed that the velocity component u scales with the local free-stream velocity, and that the radial acceleration is of the same order as the centrifugal force. This leads to:

$$u \propto \Omega r, \quad (5)$$

$$v \propto \Omega c. \quad (6)$$

Remaining scaling factors are:

$$w \propto \frac{\delta}{c}, \quad (7)$$

$$s \propto c, \quad (8)$$

$$r \propto r, \quad (9)$$

$$z \propto \delta, \quad (10)$$

in which the coordinate s replaces θ by using $r\delta\theta = \delta s$. In the following r' denotes the nondimensional radius, which is equal to one for this case. Other nondimensional parameters are used with the same symbols as the dimensional ones. Because blade sections at a distance r from the hub are considered, r has been chosen as a scaling factor. The scaling factor for q_e is the same as for u . Nondimensionalizing the equations with the scaling factors gives:

$$\frac{\partial u}{\partial s} + \left(\frac{c}{r}\right)^2 \frac{v}{r'} + \left(\frac{c}{r}\right)^2 \frac{\partial v}{\partial r'} + \frac{\partial w}{\partial z} = 0, \quad (11)$$

$$u \frac{\partial u}{\partial s} + \left(\frac{c}{r}\right)^2 v \frac{\partial u}{\partial r'} + w \frac{\partial u}{\partial z} = q_e \frac{\partial q_e}{\partial s} + \frac{1}{Re} \left(\frac{c}{\delta}\right)^2 \frac{\partial^2 u}{\partial z^2} + \left(\frac{c}{r}\right)^2 2v - \left(\frac{c}{r}\right)^2 \frac{uv}{r'}, \quad (12)$$

$$u \frac{\partial v}{\partial s} + \left(\frac{c}{r}\right)^2 v \frac{\partial v}{\partial r'} + w \frac{\partial v}{\partial z} = q_e \frac{\partial q_e}{\partial r'} + \frac{1}{Re} \left(\frac{c}{\delta}\right)^2 \frac{\partial^2 v}{\partial z^2} + \frac{u^2}{r'} - 2u. \quad (13)$$

It appears that for attached flow the ratio of the chordwise acceleration to the Coriolis force is proportional to $\left(\frac{c}{r}\right)^2$. Hence, for small c/r the influence of blade rotation will be very small. In fact it is seen that by

neglecting the terms which scale with c/r the 3-D continuity equation (11) and the chordwise momentum equation (12) are identical to the 2-D equations, and can be solved without solving the radial momentum equation.

3.1.2 Separated flow

For separated flow Snel assumed:

$$\text{Chordwise acc.} \propto \text{Coriolis force} (= \Omega v), \quad (14)$$

$$\text{Radial acc.} \propto \text{Centrifugal force} (= \Omega^2 r), \quad (15)$$

which gives:

$$u \propto \Omega r^{\frac{1}{3}} c^{\frac{2}{3}}, \quad (16)$$

$$v \propto \Omega r^{\frac{2}{3}} c^{\frac{1}{3}}. \quad (17)$$

In the equations given above the centrifugal force is hidden in the term with the edge velocity. By assuming:

$$q_e \propto \Omega r \quad (18)$$

a centrifugal force term can be recovered. Remaining scaling factors are the same as in attached flow.

The boundary layer equations now read:

$$\frac{\partial u}{\partial s} + \left(\frac{c}{r}\right)^{\frac{2}{3}} \frac{v}{r'} + \left(\frac{c}{r}\right)^{\frac{2}{3}} \frac{\partial v}{\partial r'} + \frac{\partial w}{\partial z} = 0, \quad (19)$$

$$u \frac{\partial u}{\partial s} + \left(\frac{c}{r}\right)^{\frac{2}{3}} v \frac{\partial u}{\partial r'} + w \frac{\partial u}{\partial z} = \left(\frac{c}{r}\right)^{\frac{2}{3}} q_e \frac{\partial q_e}{\partial s} + \frac{1}{Re} \left(\frac{c}{\delta}\right)^2 \frac{\partial^2 u}{\partial z^2} + 2v - \left(\frac{c}{r}\right)^{\frac{2}{3}} \frac{uv}{r'}, \quad (20)$$

$$u \frac{\partial v}{\partial s} + \left(\frac{c}{r}\right)^{\frac{2}{3}} v \frac{\partial v}{\partial r'} + w \frac{\partial v}{\partial z} = q_e \frac{\partial q_e}{\partial r'} + \frac{1}{Re} \left(\frac{c}{\delta}\right)^2 \frac{\partial^2 v}{\partial z^2} + \left(\frac{c}{r}\right)^{\frac{2}{3}} \frac{u^2}{r'} - \left(\frac{c}{r}\right)^{\frac{2}{3}} 2u. \quad (21)$$

There are still terms present in the equations which scale with c/r , but the order of magnitude is obviously less than for attached flow. If the terms which scale with c/r are neglected for small c/r , the 3-D continuity equation reduces to the 2-D equation, the chordwise momentum equation equals the 2-D equation with a Coriolis term ($2v$) added, and a radial momentum equation. So it is seen that for a separated flow the radial flow due to blade rotation will influence the chordwise flow by the Coriolis force.

3.2 Nondimensional equations

If all terms are neglected which scale with (c/r) in the equations (19) and (20) and only the first term which scales with (c/r) is neglected in equation (21), a system of equations appears which is designated the Snel model for blade rotation. This model is valid for small values of (c/r) for both attached and separated flow.



The only remaining gradient in radial direction is the gradient of the velocity at the edge of the boundary layer. However, using a proper nondimensionalization, the most important term can be captured, which eliminates the need for a discretization in radial direction. The influence of blade rotation on the chordwise flow is seen only in the Coriolis force.

Because the scaling factors for u and v in inviscid outer flow are identical to those for the attached boundary layer flow, the 2-D inviscid equations can be used. With respect to the 2-D boundary layer equations, one extra unknown (v) is added, with one additional equation. The system of equations is therefore closed.

The equations are now written into nondimensional form using the chord c as a length scale, tip radius R for the radial direction r , and $f_0 \Omega r$ as the velocity scale. The parameter f_0 determines the contribution of the rotational speed to the total freestream velocity at radius r . For a wind turbine without yaw the magnitude is given by:

$$f_0 = \sqrt{\left([1-a] \frac{R}{\lambda r} \right)^2 + (1+a')^2}, \quad (22)$$

where a and a' are the axial and circumferential induction factors, and λ the tip speed ratio. The nondimensional radial distance is denoted with r' ($=r/R$), other nondimensional symbols are identical to the dimensional symbols.

The radial derivative of the scaled velocity appears in the equations as:

$$\frac{\partial(u f_0 \Omega r)}{\partial r} = \Omega \frac{r}{R} \frac{\partial f_0 u}{\partial r'} + u f_0 \Omega. \quad (23)$$

The nondimensional equations now read:

$$\frac{\partial u}{\partial s} + \frac{\partial w}{\partial z} = 0$$

$$\left(-2 \frac{c}{r} v - \frac{c}{R} \left\{ \frac{\partial v}{\partial r'} + v \frac{1}{f_0} \frac{\partial f_0}{\partial r'} \right\} \right), \quad (24)$$

$$u \frac{\partial u}{\partial s} + w \frac{\partial u}{\partial z} = q_e \frac{\partial q_e}{\partial s} + \frac{1}{\text{Re}} \frac{\partial^2 u}{\partial z^2} + 2 \frac{c}{r} \frac{1}{f_0} v +$$

$$(+0 - \frac{c}{R} \left\{ v \frac{\partial u}{\partial r'} + \frac{1}{f_0} \frac{\partial f_0}{\partial r'} \right\}), \quad (25)$$

$$u \frac{\partial v}{\partial s} + w \frac{\partial v}{\partial z} = \frac{1}{\text{Re}} \frac{\partial^2 v}{\partial z^2} + \frac{c}{r} \left\{ q_e^2 + u \left(u - \frac{2}{f_0} \right) \right\} +$$

$$\left(-\frac{c}{r} v^2 \right.$$

$$\left. + \frac{c}{R} \left\{ q_e \frac{\partial q_e}{\partial r'} - v \frac{\partial v}{\partial r'} + (q_e^2 - v^2) \frac{1}{f_0} \frac{\partial f_0}{\partial r'} \right\} \right). \quad (26)$$

In all these three equations the Snel model for blade rotation is given on the first line, while the second line gives a higher order term which scales with c/r , and the third line gives a gradient in radial direction scaled with c/R .

It is of interest to analyze the right-hand side of the radial momentum equation. Neglecting the shear stress, it is seen that this term, given by

$$\frac{c}{r} \left\{ q_e^2 + u \left(u - \frac{2}{f_0} \right) \right\}, \quad (27)$$

is always positive (directed outwards) near the wall, and changes to the value

$$2q_e \left(q_e - \frac{1}{f_0} \right) \quad (28)$$

at the edge of the boundary layer. Taking $f_0 = 1$, and using the relation for the pressure coefficient $C_p = 1 - q_e^2$, the term becomes negative for $C_p > 0$ ($q_e < 1$), and remains positive for $C_p < 0$ ($q_e > 1$). Therefore, a radial flow directed towards the hub might occur on the pressure surface of the airfoil, and the cross-flow velocity profiles will be S-shaped.

However, here also a non-physical behaviour of the model becomes apparent: At the edge of the boundary layer $\frac{\partial v}{\partial z}, \frac{\partial^2 v}{\partial z^2} \rightarrow 0$. With $q_e \neq 1$, this is only possible when $v_e \neq 0$, which is in contradiction with the initial assumption of a 2-D inviscid flow. As the model assumes $v_e = 0$, $\frac{\partial v}{\partial z} \neq 0$ at the edge of the boundary layer, which is physically unrealistic.

The ratio $f_0 r/c$ can be interpreted as the Rossby number, which is the ratio between the inertia force and the Coriolis force:

$$\text{Ro} = \frac{[U]}{\Omega [L]} = \frac{f_0 \Omega r}{\Omega c} = \frac{f_0 r}{c}. \quad (29)$$

The parameter f_0 may be interpreted as the ratio between the centrifugal and Coriolis force, and c/r as the ratio between the centrifugal and inertia force. Within the present model, the c/r parameter can also be interpreted as the relative change in radial direction of the effective velocity:

$$\frac{c}{r} = \frac{c}{W} \frac{\partial W}{\partial r} = \frac{c}{W} \frac{W}{r}, \quad (30)$$

with $W = f_0 \Omega r$, and f_0 is assumed constant.

3.3 Exact solutions

Using the same solution procedure as for the Falkner-Skan equations, exact solutions for the velocity profile can be obtained for the 3-D boundary layer equations for a rotating blade as given by the Snel model for blade rotation:

$$\frac{u}{u_e} = f'(\eta), \quad (31)$$

$$\frac{v}{u_e} = g'(\eta), \quad (32)$$

$$\eta = z \sqrt{\frac{u_e Re}{s}}, \quad (33)$$

$$u_e = \alpha s^m. \quad (34)$$

A prime denotes a differentiation with respect to s . The nondimensional boundary layer equations may now be rewritten to:

$$f''' + m(1 - f'^2) + \frac{m+1}{2} f f'' + 2 \frac{sc}{r} \frac{1}{f_0 u_e} g' = 0, \quad (35)$$

$$g''' - m f' g' + \frac{m+1}{2} f g'' + \frac{sc}{r} \left(1 + f'^2 - \frac{2}{f_0 u_e} f' - g'^2 \right) = 0. \quad (36)$$

For $sc/r = 0$ the equations reduce to the Falkner-Skan equations. The velocity profiles on a rotating blade are no longer similar in s -direction.

Boundary conditions are for $\eta = 0$: $f = f' = g' = 0$, and for $\eta \rightarrow \infty$: $f' = 1, g' = 0$.

The equations are solved using a linearisation and finite difference scheme as given in Moran [18]. Note however that only for $f_0 u_e = 1$ the term which scales with sc/r in equation 36 goes to zero at the edge of the boundary layer, which is discussed in the previous section.

Solutions are given in figures 3 and 4 for $m = 0$ (rotating flat plate) and in figures 5 and 6 for $m = -0.09$ (near separation). All cases have been calculated with $s = 1$ and $f_0 u_e = 1$. Due to blade rotation, the velocity profile in streamwise direction becomes fuller. With increasing c/r the cross-flow increases in magnitude. The influence of blade rotation increases under the presence of an adverse pressure gradient. A similar analysis may be carried out using the Falkner-Skan model for a separated boundary layer.

4. Implementation in VII codes

The Snel boundary layer model for blade rotation was implemented in two viscous-inviscid interaction codes, suited for angles of attack up to the stall angle.

The computer code ULTRAN-V was developed at NLR by Houwink for calculating the 2-D unsteady viscous flow about airfoils in steady or unsteady motion. The code is based on the unsteady Transonic Small Perturbation (TSP) potential equation for the inviscid flow, and an integral method for the boundary layer. An unsteady version of the Green lag entrainment equation is used. Due to the strong interaction coupling between the boundary layer and the inviscid flow the applicability of the code in practice covers a wide range of subsonic and transonic, attached and separated, steady and unsteady flow conditions [11], [12] and [13]. For the radial flow additional closure relations were needed, for which the velocity profile family of Le Balleur & Lazereff [15] were used. For the

integral relations the logarithmic part was neglected. Comparison with pressure distributions measured on a wind turbine in a wind tunnel by FFA [22] showed that qualitatively the effect of blade rotation was captured well, but overpredicted in quantitative sense. In order to obtain for a rotating blade the same increase in lift due to rotational effects as measured in the experiment, the input parameter c/r had to be multiplied with a factor $2/3$.

The Snel model for blade rotation has then been implemented in the XFOIL code, developed by Drela [8], which consists of a panel method, coupled in strong interaction with an integral method for the boundary layer. Green's lag entrainment equation is used for the turbulent boundary layer. For the 3-D equations the integral equations as given by Swafford & Whitfield [29] have been adopted. For the implementation of the radial flow the cross-flow velocity profile of Johnston [14] is used:

$$\frac{v}{u_e} = \frac{u}{u_e} \tan \beta \quad (\text{near the wall}), \quad (37)$$

$$\frac{v}{u_e} = A \left(1 - \frac{u}{u_e} \right) \quad (\text{outer region}). \quad (38)$$

The inner and outer region are matched at a certain distance from the wall $\eta = y^+ = 14.1$, which gives:

$$\tan \beta_w = A \left(\frac{1}{\eta \left(\frac{C_{f1}}{2} \cos \beta_w \right)^{\frac{1}{2}}} - 1 \right). \quad (39)$$

Using only the relation for the outer region, the cross-flow integral quantities are easily rewritten into chordwise integral quantities and the cross-flow parameter A . The relations are given by Swafford & Whitfield. The radial dissipation coefficient, present in the kinetic energy equation, has been rewritten as a summation of an inner layer, for which the formulation as given by Thomas [30] is used, and an outer layer, which can be related to the chordwise dissipation coefficient using the Johnston velocity profile, assuming isotropic eddy viscosity. No cross-flow corrections have been made in the Green lag entrainment formulation. The modified code has been named RFOIL. The integral relations for the chordwise and radial momentum equations may now be written as:

$$\begin{aligned} I & \frac{s}{\theta_{11}} \frac{\partial \theta_{11}}{\partial s} = \frac{s}{\theta_{11}} \frac{C_{f1}}{2} - (H+2) \frac{s}{u_e} \frac{\partial u_e}{\partial s} \\ I & - \frac{c}{r} \frac{2s}{f_0 u_e} H A \\ II & + \frac{sc}{r} 2A(2-H) \\ IV & + \frac{sc}{R} \frac{1}{f_0 u_e} \frac{\partial (f_0 u_e)}{\partial r} A(2-H) \\ V & - \frac{sc}{\theta_{11} R} \frac{\partial \theta_{21}}{\partial r} + \frac{sc}{\theta_{11} R} \frac{\partial \delta_2^*}{\partial r} \end{aligned} \quad (40)$$

$$I \quad -s \frac{\partial A}{\partial s} - A \frac{s}{\theta_{11}} \frac{\partial \theta_{11}}{\partial s} = \frac{s}{\theta_{11}} \frac{C_{f2}}{2} + 2A \frac{s}{u_e} \frac{\partial u_e}{\partial s}$$

$$\begin{aligned}
 I & -\frac{sc}{r} \left(2H_1 \left(1 - \frac{1}{f_0 u_e} \right) + H - 1 \right) \\
 II & +\frac{sc}{r} (H - 1) 3A^2 \\
 III & -\frac{sc}{R} (H_1 + H) \frac{1}{f_0 u_e} \frac{\partial f_0 u_e}{\partial r} \\
 IV & -\frac{sc}{R} 2A^2 (1 - H) \frac{1}{f_0 u_e} \frac{\partial f_0 u_e}{\partial r} \\
 V & -\frac{sc}{\theta_{11} R} \frac{\partial \theta_{22}}{\partial r} \quad (41)
 \end{aligned}$$

where the complete 3-D integral equations are now each divided into several parts:

- I. equation as derived from simplified boundary layer equations (Snel formulation) without the radial nondimensional pressure coefficient gradient
- II. extra terms, which can be implemented easily in the present Snel model: curvature terms and terms which arise due to nondimensionalization of the gradients in radial direction with the rotational speed. All these terms scale with c/r .
- III. radial nondimensional pressure coefficient gradient which is present in the Snel formulation, hence leading order term. This term is the gradient in the right hand side of equation (23), where the radial pressure gradient has been split in two components.
- IV. remaining (higher order) terms of radial nondimensional pressure coefficient gradient.
- V. radial gradients of integral quantities.

Only term I was implemented in the ULTRAN-V code, while all terms have been implemented in the RFOIL code. The 3-D kinetic energy equation is a rather lengthy formulation which can be found in [29]. Note that the used cross-flow velocity profiles are not able to model an S-shaped profile.

5. Steady calculations

Calculations using the ULTRAN-V and RFOIL code will be discussed and compared with experimental results and a Navier-Stokes solution. The influence of velocity variations and transition is also discussed.

5.1 Influence of blade rotation

The effect of blade rotation on the pressure distribution and boundary layer characteristics is discussed first. A calculation has been made using the RFOIL code for a NACA 4415 airfoil with blunt trailing edge, using 120 panels on the airfoil. Only terms I and II as given above have been used. The calculations have been made using fixed transition at 10% chord. Results for different c/r values are presented in figure 7. The value $c/r = 0$ represents the non-rotating

case. With increasing c/r value the separation point appears to move towards the trailing edge, which can be observed in the chordwise skin friction coefficient. Furthermore the pressure distribution in the separated flow region is no longer flat, but shows a small gradient. The increase in chordwise displacement thickness is reduced due to the Coriolis force. At the leading edge a small laminar separation bubble is present. On the upper surface there is an increase in skin friction, whereas on the lower surface the skin friction is decreased in value. Analysis of the results shows that from the stagnation point onwards on the upper surface, the radial displacement coefficient is positive for 5 % chord lengths, after which it becomes negative. On the lower surface, however, the radial displacement thickness remains positive from the stagnation point to the trailing edge. The radial displacement thickness has a negative value for an outward directed flow. Therefore the average flow at the leading edge on the upper surface, and on the entire lower surface is directed inwards. Near the wall the radial flow should be directed outwards, which gives a positive Coriolis force, and therefore the skin friction should increase. Due to the inability of the used cross-flow model to model S-shaped velocity profiles, this is not possible, and a decrease in skin friction is seen. It is also seen that the cross-flow displacement thickness on the upper surface varies linearly, whereas the ULTRAN-V results presented in [27] showed a quadratic increase in the cross-flow displacement thickness. This is explained by the addition of term II in the radial momentum equation, which damps the growth of the cross-flow.

Although it is recognized that the Prandtl boundary layer assumption is no longer valid beyond the static stall angle, it will still be used here from an engineering point of view.

5.2 Influence of higher order terms

The higher order terms III, IV and V have been implemented as explicitly given source terms. From two neighbouring sections the radial gradients were calculated and stored in an additional input file. The sections were then recalculated with the additional terms included. Term III appeared to change the radial flow significantly in separated flow. However, as the radial flow is only affected by the chordwise flow through the Coriolis force, the influence on the chordwise displacement thickness and lift coefficient was very small. Including the higher order terms IV and V did not change the solution for attached flow, as expected. Unfortunately, due to convergence problems, no solution has been obtained for separated flows.

5.3 Comparison with experiment

There is only a limited amount of good experimental data sets available which can be used for valida-

tion purposes. Most data for wind turbines have been measured on open air facilities, with all the unsteady variations in the wind velocity and direction included. Wind tunnel data of a rotating blade are available by the FFA measurements in the CARDC wind tunnel, located in China, including pressure distributions. The blades were also measured in non-rotating conditions in an FFA tunnel. The rotor blades had a length of 2.375 meter, and were equipped with NACA 44xx airfoils. Thickness varied from 22% chord at 30% radius to 14% chord at the tip. The blades, test campaign and analysis of the data are described in [4], [22] and [23]. At 30% radius of the rotating blade a large increase in lift coefficient was measured compared to the non-rotating test, and at 55% a small increase. At the tip the maximum lift was lower compared to the non-rotating test. For the present calculations only the airfoil section at 55% radius was used, with a fixed transition point and a Reynolds number of 0.5E6. Angles of attack for the non-rotating case were calculated by FFA using a lifting line method. For the rotating case, a local blade element momentum theory was used to give an estimate of the angle of attack. The analysis is reported by Snel [26]. Calculated results will be shown using both ULTRAN-V and RFOIL.

Some representative pressure distributions are presented in figure 8 for the 55% section nonrotating, figure 9 for the 55% section rotating, and in figure 10 for the 30% section rotating. For ULTRAN-V the upper and lower surface pressure distribution have been plotted separately; ls stands for lower surface. All angles of attack are approximately 21 deg. For the rotating case the c/r used in the calculations was the geometric value of the section multiplied with a correction factor of 2/3. Both calculations and experiment show a flat pressure distribution in the separated flow region for the non-rotating case, and a linear increase in pressure in the separated flow region for the rotating case. The linear change in the separated flow region is larger for the 30% section than for the 55% section. Largest differences between calculations and experiment are found in the leading edge region, indicating inaccuracy in modelling.

5.4 Comparison with Navier-Stokes results

A comparison has been made with a 3-D Navier-Stokes solver, developed by Hansen of the Technical University of Denmark [10]. The airfoil used is an NLF-0416 airfoil as used on the open air facility of the TU Delft [6]. A rather coarse grid was applied, and the turbulence model was tuned in a 2-D calculation in order to obtain the same maximum lift coefficient as measured in a 2-D wind tunnel experiment. Figure 11 shows the results of the 2-D calculations and the 3-D calculations. For the ULTRAN-V calculation the c/r ratio was again reduced with a factor 2/3. Both codes show very similar results. Due to blade rotation the flat pressure distribution in separated flow no longer

exists, and an increase in pressure peak at the leading edge is seen. Both codes show a forward movement of the separation point due to blade rotation, as seen in the forward movement of the kink in the pressure distribution. The calculations on the NACA 4415 airfoil showed however a delay in the forward movement of the separation point. At present, other airfoils have not been investigated.

5.5 Influence on lift

Comparison of RFOIL and ULTRAN-V data with experimental results of FFA and ECN showed that the c/r input value had to be multiplied with 2/3 in order to obtain the same increase in lift on a rotating blade section with respect to a non-rotating blade section. The neglect of the radial gradients of integral quantities in the used boundary layer equations is probably the reason for this. Also the used cross-flow velocity profile might be inadequate for large separated flow regions, as known validations only consider attached and slightly separated flow.

The increase in lift coefficient due to blade rotation is shown in figure 12. A comparison is made with the non-rotating data of FFA as measured at the 55% section. The RFOIL code is not able to predict the flow well after the static stall point, where the drop in lift coefficient is too small, due to the large suction peak at the nose. The difference between RFOIL and ULTRAN-V is shown in figure 13. There is a good agreement for the large c/r value, while for the low c/r value the agreement is less due to the different behaviour in the 2-D calculation. ULTRAN-V shows a much larger decrease in lift after the stall point than RFOIL. In contrary to ULTRAN-V results, RFOIL calculations suggest that after a certain angle of attack the increase in lift remains constant. Because convergence problems prohibited the calculation of higher angles of attack, this can not be substantiated.

On the basis of the ULTRAN-V calculations a first crude correction factor for the effect of blade rotation was devised by Houwink and Snel [26] which is given by:

$$c_{l3D} = c_{l2D} + 3(c/r)^2 (c_{l\text{inviscid}} - c_{l2D}). \quad (42)$$

5.6 Influence of velocity variation

The freestream velocity W (effective wind velocity as seen by blade section) may vary in two ways in the model. The absolute variation is seen as a Reynolds number effect. The relative contribution of the rotational speed and the wind speed is brought into the model by the f_0 parameter.

The effect of a varying Reynolds number is considered first. With increasing Reynolds number viscous effects will become less dominant. Therefore with increasing Reynolds number the radial flow will be less, and the increase in lift due to blade rotation will also be less. The delta values (3-D value minus 2-D value)

are shown in figure 14. With increasing Reynolds number the increase in lift is less, the decrease in drag is less, and also the separation point is less delayed. At the larger angles of attack the delta value starts to decrease.

The influence of a variation in the f_0 parameter appears to be negligible on the lift coefficient for the range of values occurring at wind turbines without yaw, where f_0 varies between 1 and 1.3. The effect of an increase in f_0 is shown in figure 15. A small increase in f_0 gives a larger cross-flow when the flow is attached, but decreases the cross-flow in separated flow regions. Due to the increase in the attached flow the chordwise displacement thickness is reduced, and the lift has slightly increased. For values larger than 2 the lift coefficient decreases noticeably.

5.7 Influence of transition

So far only the influence on the lift coefficient has been considered, with the transition point fixed at the nose. In case of free transition the effect of blade rotation will be more complicated because transition might occur due to the cross-flow. The inflection point in the cross-flow velocity profile might lead to an unstable situation. Arnal [1] investigated cross-flow transition due to a yawed flow, and gave a criterion based upon the cross-flow displacement thickness Reynolds number and the shape factor.

As the model of Arnal has not been implemented yet, only exploratory calculations using the RFOIL code will be shown. Figure 16 shows a 2-D calculation with free transition, and 2-D and 3-D calculations with transition fixed at 1% upper surface and 50% lower surface. By fixing the transition at the leading edge the maximum lift coefficient is reduced in value for a non-rotating blade. For small values of c/r the reduction in maximum lift due to a moving transition point is larger than the increase in lift due to blade rotation. The drag coefficient increases due to early transition for the rotating section and small angles of attack, until the pressure drag starts to dominate the drag coefficient. The behaviour of the moment coefficient is also shown in figure 16. The moment coefficient on a rotating blade is more negative. However, as it was noticed already that the leading edge suction peak is too large in the calculations, the calculated moment coefficient at the higher angles of attack is not considered reliable.

6. Unsteady calculations

The Snel boundary layer formulation for unsteady effects has been extended with the time-dependent terms in the ULTRAN-V code. The most interesting case would be to calculate a dynamic stall loop, with angles of attack well above the static angle of attack. However, the ULTRAN-V code is unable to simulate the dynamic stall vortex which characterizes the deep dynamic stall loops, due to the integral formulation of

the boundary layer equations. Therefore only a case with light stall will be shown, in which some separation is present. As a reference for the 2-D calculations, the NACA 0015 airfoil experiment by Piziali is used [21]. Test conditions were $Re = 2.E6$, $Mach = 0.3$ and transition fixed at 10 % chord. Comparison with experimental data showed that the calculated hysteresis loop was too large.

The influence of blade rotation on the unsteady lift variation is shown in figure 17. It is seen that during the upstroke the unsteady effects delay separation and rotational effects are small. After separation at the end of the upstroke, the flow remains separated during part of the downstroke and consequently is more sensitive to rotational effects. The maximum lift has increased, and the hysteresis loop has decreased in magnitude.

7. Concluding remarks

The Snel model for blade rotation has been implemented in an airfoil analysis code, consisting of a panel method describing the inviscid flow coupled in strong interaction with an integral method for the boundary layer. The new code was designated RFOIL. Previously the model has been implemented into the airfoil analysis code ULTRAN-V by Houwink [27], and results showed that qualitatively the effect of blade rotation was well predicted, but the input c/r value had to be multiplied with 2/3 in order to obtain quantitative correlation. Comparison of RFOIL results with ULTRAN-V results, experimental data of FFA and a 3-D Navier-Stokes solution of Hansen [10] showed that due to the Coriolis force in chordwise momentum thickness the chordwise displacement thickness is reduced in separated flow, giving a linear increase in pressure instead of the constant pressure observed in separated flow on a non-rotating blade. However, despite the addition of some extra terms to the Snel model for blade rotation in the RFOIL code, the correction factor of 2/3 to the c/r value still had to be applied. Possible reasons for this correction factor include:

- Radial gradients of the boundary layer integral quantities have not been taken into account, because of numerical convergence problems at angles of attack where the flow starts to separate.
- The used cross-flow velocity profiles in ULTRAN-V and RFOIL have not been validated for the large separated flow regions which have been calculated.
- It was shown using the Snel model for blade rotation that a cross-flow should also occur in the inviscid outer flow. This velocity component has been neglected.
- The calculated suction peak at the leading edge is too large compared with experimental data.

The calculated influence of blade rotation on the separation point was dependent on the airfoil: For a NACA 4415 airfoil separation was delayed, but for a NLF0416 airfoil separation was enhanced.

A topic which has been addressed briefly is the influence of transition. Transition may be enhanced due to the cross-flow, which causes a decrease in maximum lift and an increase in skin friction drag. This complicates the effect of blade rotation, which was initially thought to only increase lift and decrease drag for inboard sections. The calculated effect of blade rotation on the moment coefficient should be considered with some care due to the large suction peaks at the leading edge.

It has also been noticed that due to blade rotation S-shaped cross-flow velocity profiles might occur in the boundary layer, which can not be modelled by the used cross-flow velocity profiles.

In practice, the effect of blade rotation is combined with a cross-flow velocity component in the inviscid flow due to yaw-misalignment of the wind turbine or a forward flight motion of the helicopter. This complicated issue has not been addressed yet, but needs more attention.

The final conclusion is that there is a need for more accurate boundary layer data for separated flows on rotating blades, obtained either by experiment or by 3-D calculations methods.

8. References

- [1] D. Arnal. Three-dimensional boundary layers: laminar-turbulent transition. AGARD R741: Computation of 3-D boundary layers including separation, 1987.
- [2] W.H.H Banks and G.E. Gadd. Delaying effect of rotation on laminar separation. *AIAA journal*, Vol. 1, no 4., April 1963.
- [3] J. Bessone and D. Petot. Evaluation de modes aerodynamiques et dynamiques des rotors d'helicopteres par confrontation a l'experience. AGARD symposium on Aerodynamics and Aeroacoustics of Rotorcraft, 1994.
- [4] A. Bjorck, G. Ronsten, and B. Montgomerie. Aerodynamic section characteristics of a rotating and non-rotating 2.375 m wind turbine blade. Technical Report TN 1995-03, FFA, 1995.
- [5] A.J. Brand, J.W.M. Dekker, C.M. de Groot, and M. Späth. Aerodynamic field data from the HAT25 experimental wind turbine. Technical Report C-96-037, ECN, 1996.
- [6] A. Bruining, G.J.W. van Bussel, G.P. Corten, and W.A. Timmer. Pressure distributions from a wind turbine blade; field measurements compared to 2-dimensional wind tunnel data. Technical Report IW-93065R, IVW, Delft University of Technology, 1993.
- [7] J.J. Corrigan and J.J. Schillings. Empirical model for stall delay due to rotation. AHS Aeromechanics specialists conference, 1994.
- [8] M. Drela. XFOIL: an analysis and design system for low Reynolds number airfoils. Conference on Low Reynolds number aerodynamics, Lecture Notes in Engineering 54, Notre Dame. Springer Verlag., June 1989.
- [9] L.E. Fogarty. The laminar boundary layer on a rotating blade. *J. Aero. Science*, Vol. 18, no 4., 1951.
- [10] M.O.L. Hansen, J.A. Michelsen, and N.N. Sørensen. Computed 3D effects on a rotating wind turbine blade. EUWEC 1996, Göteborg.
- [11] R. Houwink. Computation of unsteady turbulent boundary layer effects on unsteady flow about airfoils. Technical Report TP 89003, NLR, 1989.
- [12] R. Houwink, J.A. van Egmond, and P.A. van Gelder. Computation of viscous aerodynamic characteristics of 2-D airfoils for helicopter applications. Technical Report MP 88052, NLR, 1988.
- [13] R. Houwink and A.E.P. Veldman. Steady and unsteady separated flow computations for transonic airfoil. AIAA 84-1618, 1984.
- [14] J.P. Johnston. On the three-dimensional turbulent boundary layer generated by secondary flows. *J. Basic Eng. Vol 82, ASME Series D pp 233-248*, 1960.
- [15] M. Lazareff and J.C. Le Balleur. Calcul d'écoulement tridimensionnels par interaction visqueux-non visqueux utilisant la methode MZM. AGARD CP 412, 1986.
- [16] W.J. McCroskey. Recent developments in rotor blade stall. AGARD CP 111, 1973.
- [17] B. Montgomerie, A. Brand, R. van Rooij, and J. Bosschers. Three-dimensional and rotational effects on the boundary layer and consequences for wind turbine rotors. EUWEC, 1996, Göteborg.
- [18] J. Moran. *An introduction to theoretical and computational aerodynamics*. John Wiley & Sons, Inc., 1984.
- [19] J.C. Narramore and R. Vermeland. Navier-Stokes Calculations of Inboard Stall Delay due to Rotation. *Journal of Aircraft*, volume 29, no. 1, Jan.-Feb. 1992.
- [20] R.J.H. Paynter and J.M.R. Graham. Blade surface pressure measurements on an operating wind turbine. EUWEC 1996, Göteborg.
- [21] R.A. Piziali. 2D and 3D oscillating wing aerodynamics for a range of angles of attack including stall. Technical Report TM-4632, NASA, 1994.



- [22] G. Ronsten. Static pressure measurements on a rotating and a non-rotating 2.375 m wind turbine blade. comparison with 2D calculations. European Wind Energy Conference, Amsterdam, 1991.
- [23] G. Ronsten. Geometry and installation in wind tunnels of a STORK 5.0 WPX wind turbine blade equipped with pressure taps. Technical Report FFAP-A 1006, FFA, 1994.
- [24] H. Schlichting. *Boundary layer theory*. McGraw-Hill, 1979.
- [25] H. Snel. Scaling laws for the boundary layer flow on rotating wind turbine blades. IEA symposium on the aerodynamics of wind turbines, 1990, Rome.
- [26] H. Snel, R. Houwink, and J. Bosschers. Sectional Prediction of Lift Coefficients on Rotating Wind Turbine Blades in Stall. Technical Report ECN-C-93-052, Netherlands Energy Research Foundation ECN, 1994.
- [27] H. Snel, R. Houwink, and W.J. Piers. Sectional Prediction of 3D Effects for Separated Flow on Rotating Blades. 18th European Rotorcraft Forum, 1992. Also published as NLR TP92409.
- [28] J.N. Sørensen. Prediction of three-dimensional stall on wind turbine blade using three level viscous-inviscid interaction model. EWEC, 1986, Rome.
- [29] T.W. Swafford and D.L. Whitfield. Time-dependent solution of three-dimensional compressible turbulent integral boundary-layer equations. *AIAA Journal*, Vol. 23, No. 7, July 1985.
- [30] J.L. Thomas. Integral boundary layer models for turbulent separated flows. AIAA-84-1615, 1984.
- [31] R.P.J.O.M. van Rooy. Modification of the boundary layer calculations in RFOIL for improved air-foil stall prediction. Technical Report IW-96101R, Delft University of Technology, 1996.
- [32] Z.U.A. Warsi. *Fluid dynamics: theoretical and computational approaches*. CRC Press, 1993.

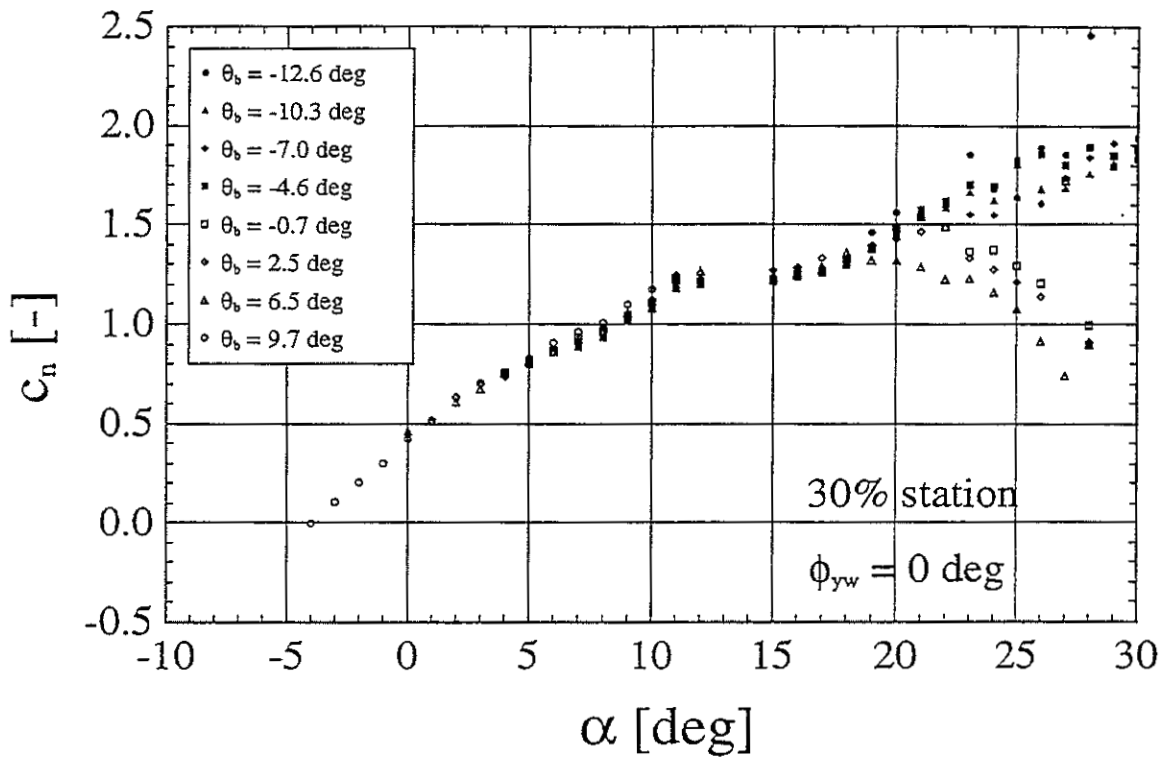


Figure 1: Normal force coefficients measured by ECN at the 30% radius section

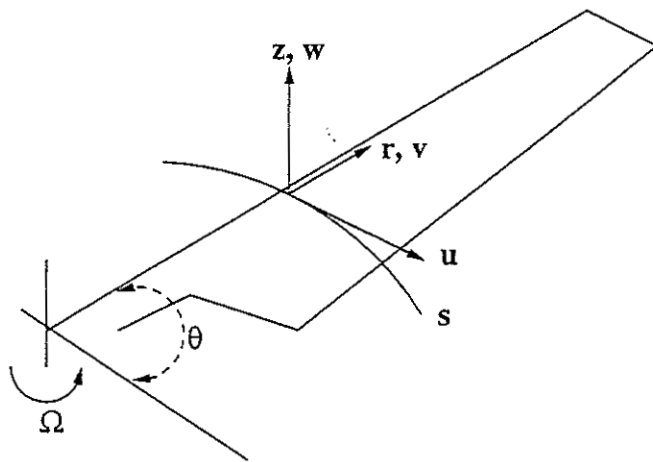


Figure 2: The coordinate system

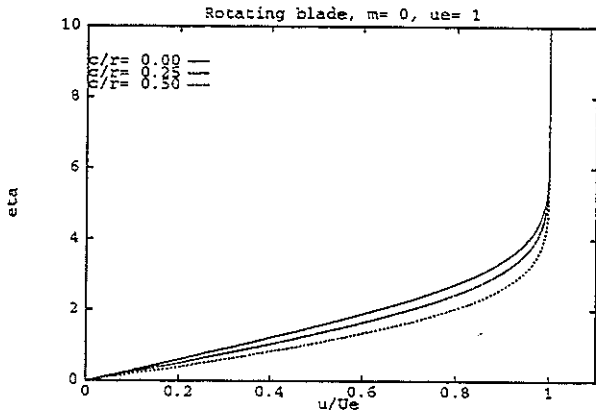


Figure 3: Streamwise velocity profiles for zero pressure gradient

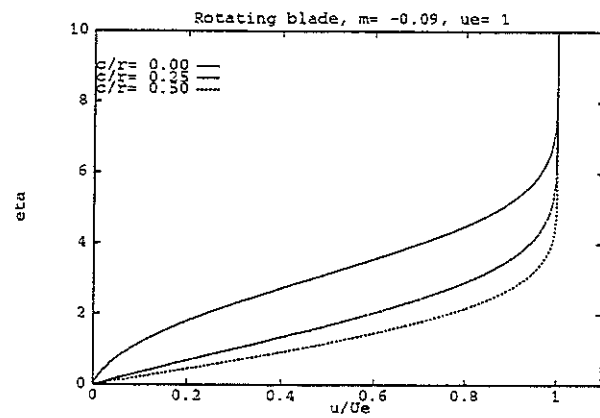


Figure 5: Streamwise velocity profiles with pressure gradient $U_e = \alpha s^{-0.09}$

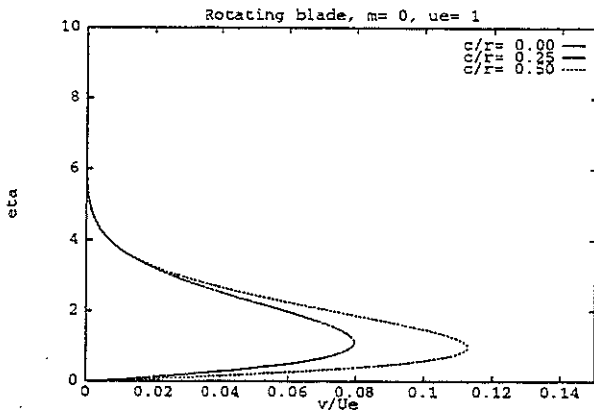


Figure 4: Cross-flow velocity profiles for zero pressure gradient

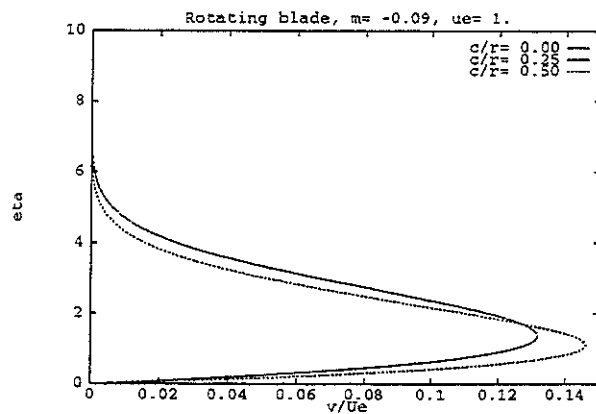


Figure 6: Cross-flow velocity profiles with pressure gradient $U_e = \alpha s^{-0.09}$



<i>FFA rotor 55% section</i>	— $c/r = 0.0$
<i>RFOIL V1.0</i>	- - - $c/r = 0.11$
$Re = 5.85$	- - - $c/r = 0.25$
$\alpha = 20.0 \text{ deg}$	
$xtr = (0.1, 0.1)$	

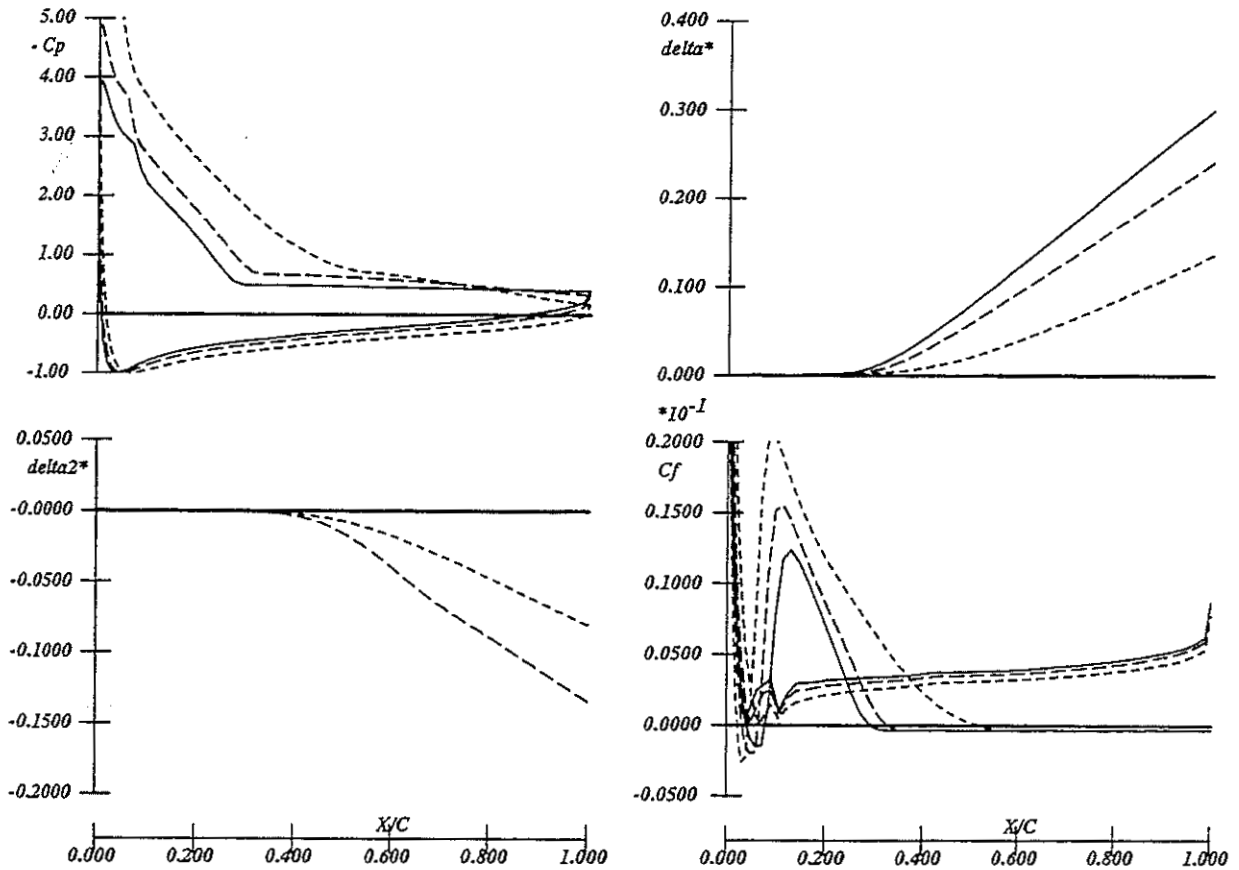


Figure 7: Influence of blade rotation at $\alpha = 20 \text{ deg}$, calculated with RFOIL

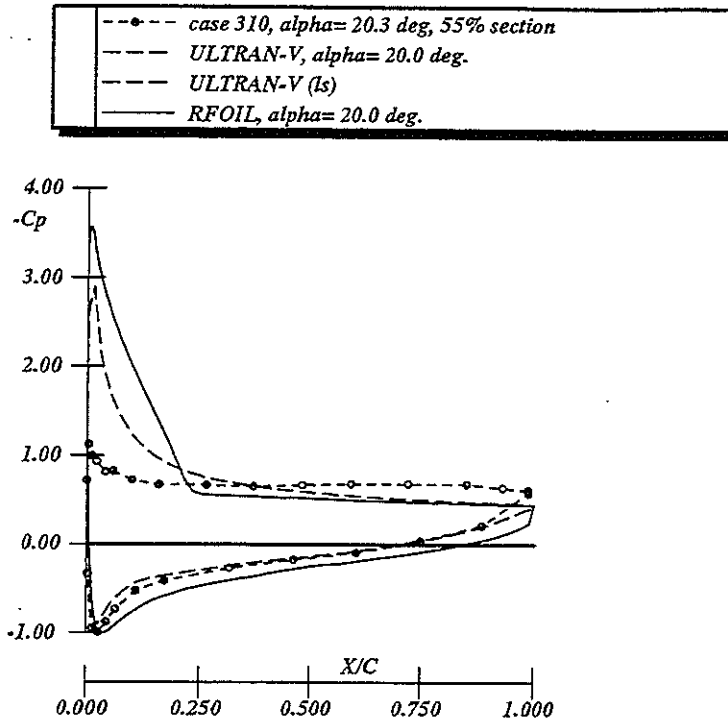


Figure 8: Comparison between 2-D model and nonrotating FFA data at $Re= 5.E5$

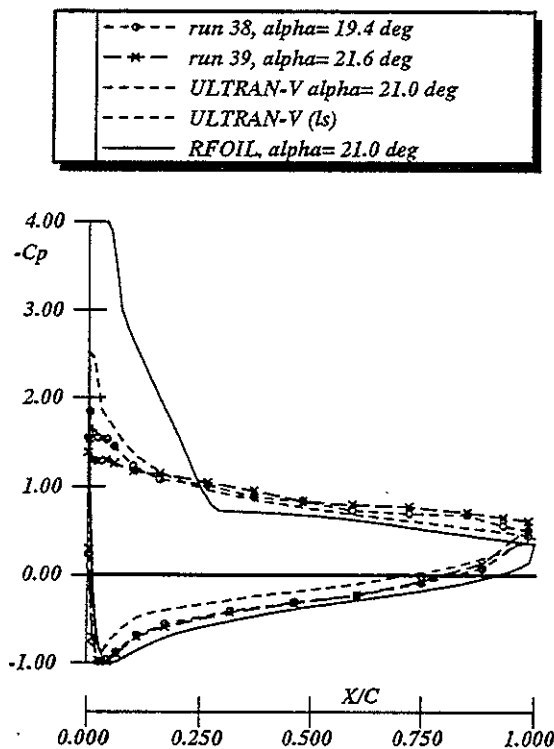


Figure 9: Comparison between quasi 3-D models and FFA data at 55% section at $\alpha \approx 21$ deg

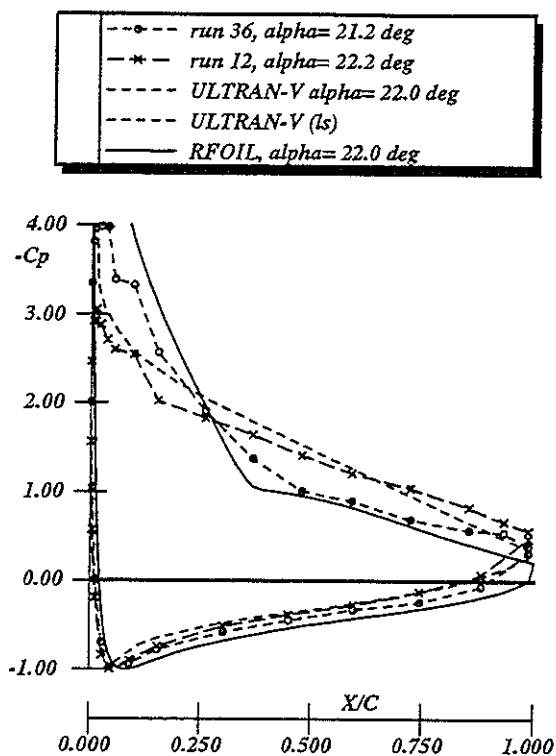


Figure 10: Comparison between quasi 3-D models and FFA data at 30% section at $\alpha \approx 22$ deg

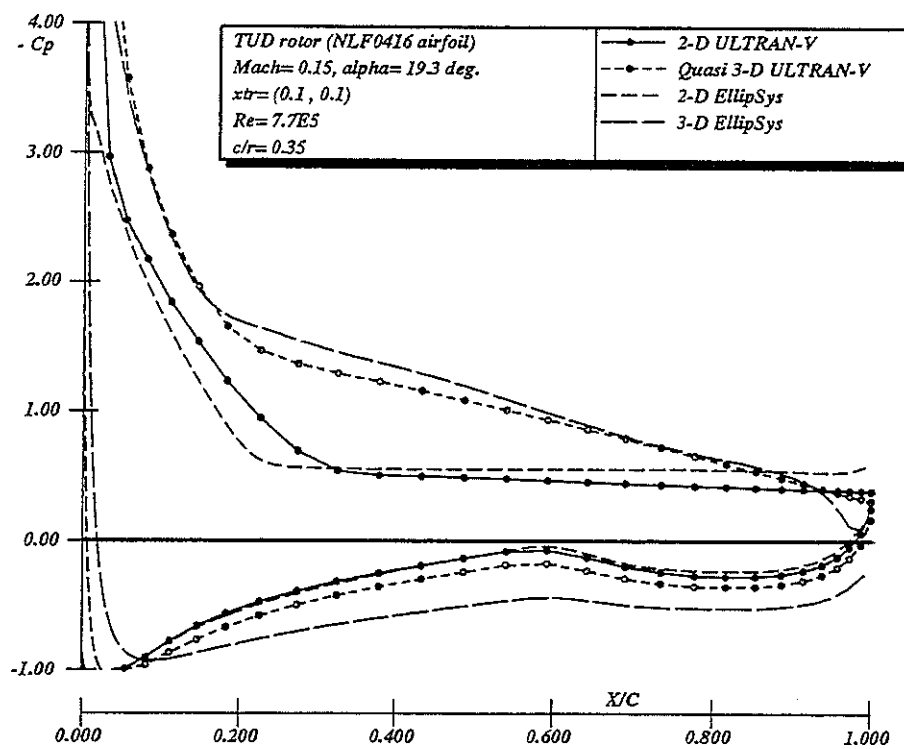


Figure 11: Comparison in results between ULTRAN-V and the 3-D Navier-Stokes solver EllipSys



<i>FFA rotor 55% section</i>	— RFOIL 2D
<i>Re= 5.E5</i>	- - - RFOIL c/r= 0.11
<i>xtr= (0.1,0.1)</i>	- - - RFOIL c/r= 0.25
<i>Rfoil V1.0</i>	o EXP 55% 2D
	x EXP 55%, c/r= 0.16
	▲ EXP 30%, c/r= 0.37

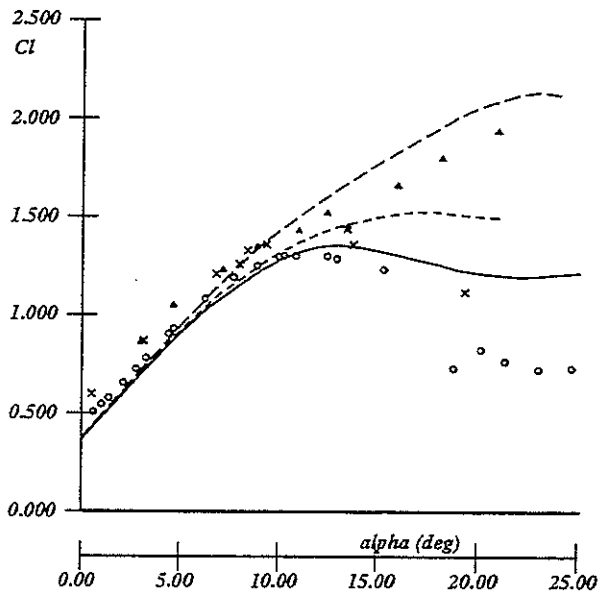


Figure 12: Influence of blade rotation on lift coefficient, calculations compared with measurements

<i>Lift increase</i>	— RFOIL c/r= 0.11
<i>FFA rotor 55% section</i>	- - - RFOIL c/r= 0.25
<i>Re= 5.E5</i>	o ULTRANV c/r= 0.11
<i>fixed transition</i>	o ULTRANV c/r= 0.25

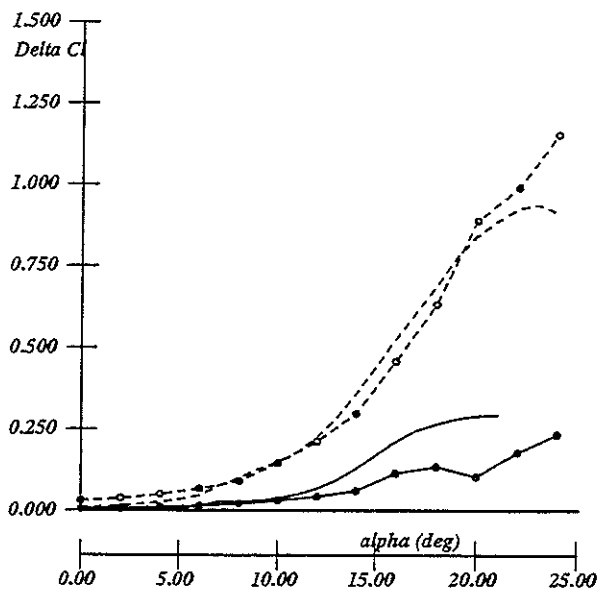


Figure 13: Comparison between RFOIL and ULTRAN-V of the increase in lift coefficient due to blade rotation



Lift increase	— $Re=0.5E6$
FFA 55% HAT section	- - - $Re=1.0E6$
$c/r=0.2$	- - - $Re=2.0E6$
fixed transition	

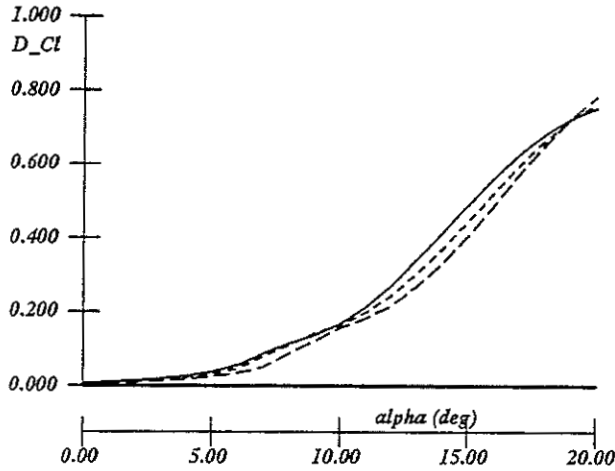


Figure 14: Calculated increase in lift coefficient due to blade rotation

FFA rotor 30% section	— $f_0=1.0$
$\alpha = 14$ deg.	- - - $f_0=1.2$
$Re=0.5E6, c/r=0.2$	
$xtr=(0.01, 0.5)$	

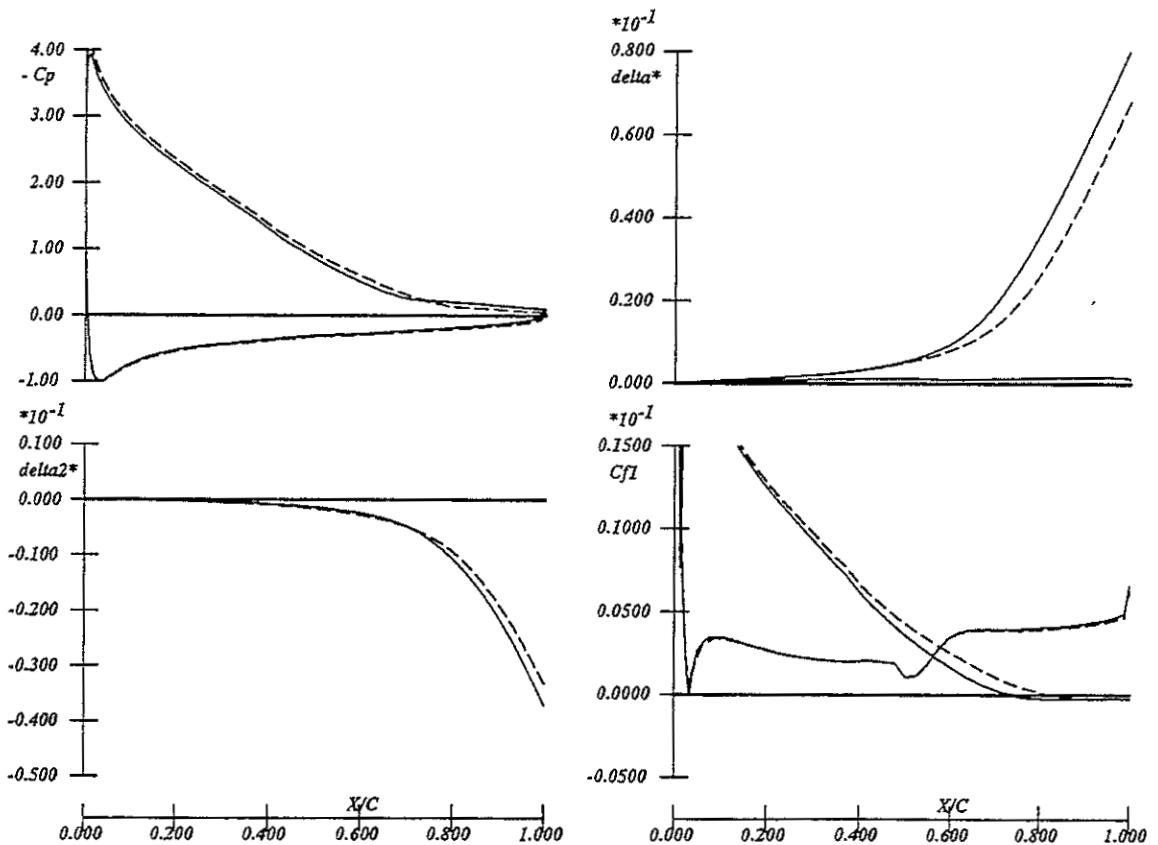


Figure 15: Calculated influence of increase in f_0 parameter at $\alpha = 14$ deg

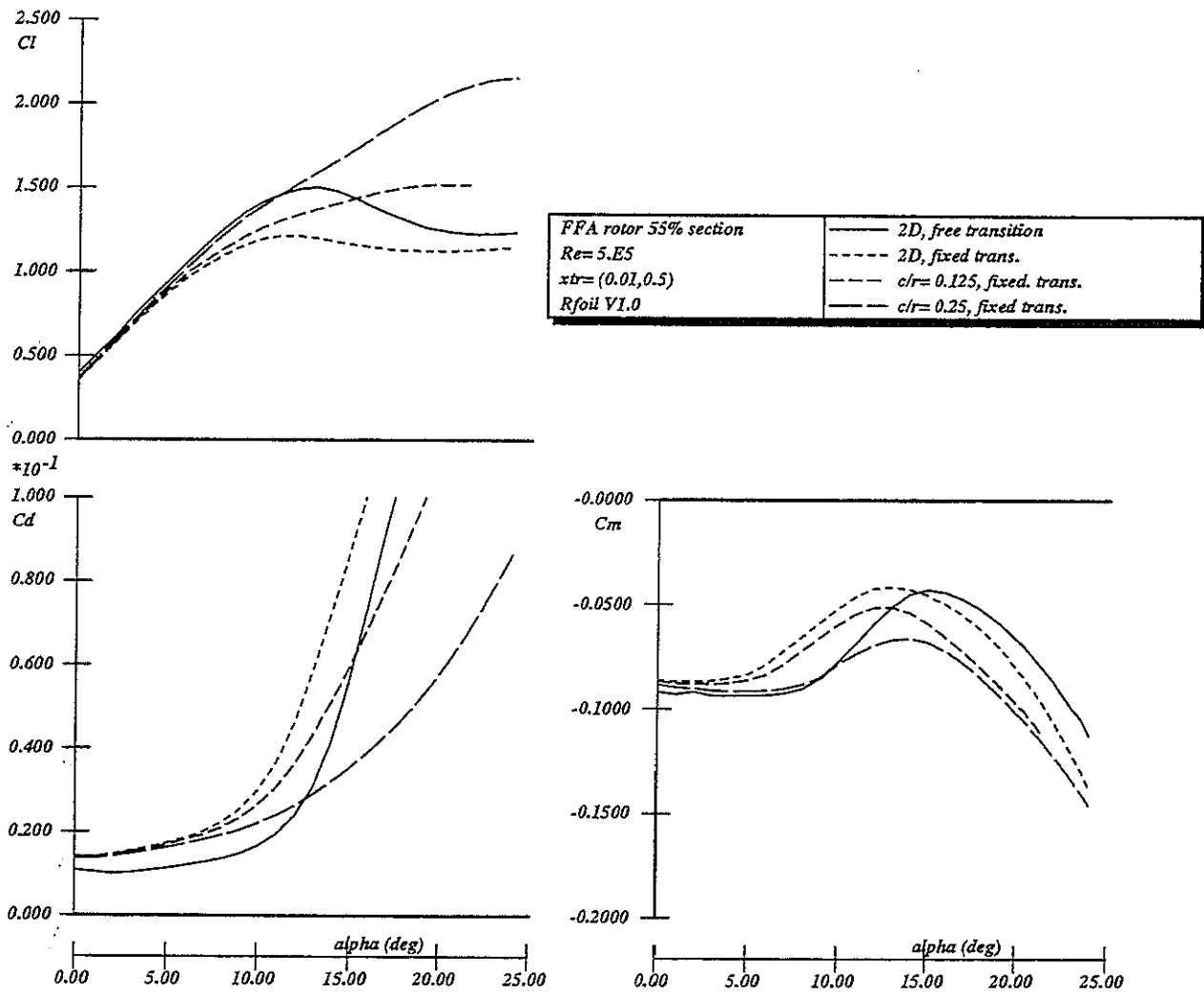


Figure 16: Calculated influence of blade rotation



NACA 0015	— c/r= 0.00, steady
ULTRAN-V code	- - - c/r= 0.15, steady
$\alpha = 11 + 4.2 \sin(\psi)$	— c/r= 0.00
$M = 0.3, Re = 1.E6, k = 0.05$	- - - c/r= 0.15
tripped at (0.1,0.1)	

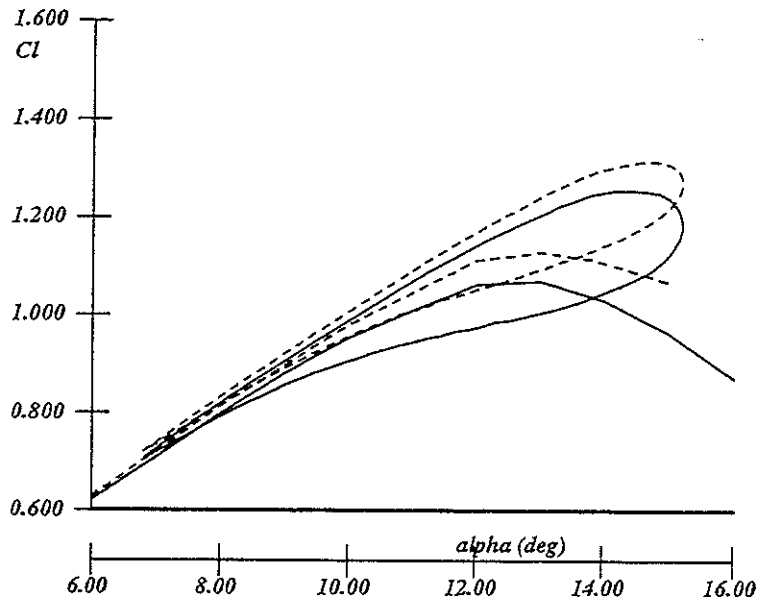


Figure 17: Calculated influence of blade rotation of a pitching airfoil in light stall